## Rheology of Candida albicans fungal biofilms

Joanne K. Beckwith, Mahesh Ganesan, J. Scott VanEpps, et al.

Citation: Journal of Rheology 66, 683 (2022); doi: 10.1122/8.0000427

View online: https://doi.org/10.1122/8.0000427

View Table of Contents: https://sor.scitation.org/toc/jor/66/4

Published by the The Society of Rheology

## ARTICLES YOU MAY BE INTERESTED IN

Extensional rheology and flow-induced crystal alignment in polypropylene ionomers Journal of Rheology **66**, 657 (2022); https://doi.org/10.1122/8.0000404

Rheology and microstructure of discontinuous shear thickening suspensions Journal of Rheology **66**, 731 (2022); https://doi.org/10.1122/8.0000317

Linear viscoelasticity of PP/PS/MWCNT composites with co-continuous morphology Journal of Rheology **66**, 671 (2022); https://doi.org/10.1122/8.0000441

DNA topology dictates emergent bulk elasticity and hindered macromolecular diffusion in DNA-dextran composites

Journal of Rheology 66, 699 (2022); https://doi.org/10.1122/8.0000447

Nonlinear rheology of entangled wormlike micellar solutions predicted by a micelle-slip-spring model Journal of Rheology **66**, 639 (2022); https://doi.org/10.1122/8.0000426

Imaging of the microstructure of Carbopol dispersions and correlation with their macroelasticity: A micro- and macrorheological study

Journal of Rheology 66, 749 (2022); https://doi.org/10.1122/8.0000452

DISCOVER the RHEOMETER with the...

Sensitivity • Ease-of-use • Versatility

to address the most demanding applications

The **NEW Discovery Hybrid Rheometer** 



# Rheology of Candida albicans fungal biofilms

Joanne K. Beckwith, <sup>1,2,a)</sup> Mahesh Ganesan, <sup>1,2</sup> J. Scott VanEpps, <sup>2,3,4,5,6</sup> Anuj Kumar, <sup>7</sup> and Michael J. Solomon<sup>1,2</sup>

<sup>1</sup>Department of Chemical Engineering, University of Michigan, Ann Arbor, MI 48109
<sup>2</sup>Biointerfaces Institute, University of Michigan, Ann Arbor, MI 48109
<sup>3</sup>Department of Emergency Medicine, University of Michigan, Ann Arbor, MI 48109
<sup>4</sup>Department of Biomedical Engineering, University of Michigan, Ann Arbor, MI 48109
<sup>5</sup>Macromolecular Science and Engineering, University of Michigan, Ann Arbor, MI 48109
<sup>6</sup>Michigan Center for Integrative Research in Critical Care, University of Michigan, Ann Arbor, MI 48109
<sup>7</sup>Department of Molecular, Cellular, and Developmental Biology, University of Michigan, Ann Arbor, MI 48109

(Received 22 December 2021; final revision received 20 April 2022; published 24 May 2022)

#### **Abstract**

Fungi such as *Candida albicans* exist in biofilm phenotypes, which present as viscoelastic materials; however, a method to measure linear viscoelastic moduli, yield stress, and yield strain is lacking. Characterization methods for fungal materials have been limited to techniques specific to particular industries. Here, we present a method to measure the shear stress, strain amplitude, and creep of *C. albicans* BWP17 biofilms. Our method includes features tailored to the analysis of fungi including an *in vitro* growth protocol attuned to the slow growth rates of *C. albicans* biofilms and a resultant cultured biofilm that has sufficient integrity to be transferred to the rheometer tooling without disrupting its structure. The method's performance is demonstrated by showing that results are insensitive to gap, evaporative sealant, length of experiment, and specimen radius. Multiscale imaging of the fungal biofilm showed complex entanglement networks at the hundred-micrometer scale. For a wild-type strain cultivated for 14 days, using small-amplitude oscillatory rheology, we found that the elastic (G') and viscous (G'') moduli were nearly independent of frequency over the range  $0.1-10\,\mathrm{s}^{-1}$ , with magnitudes of  $18\,400\,\pm\,1100$  and  $1700\,\pm\,140\,\mathrm{Pa}$ , respectively. The yield stress was approximately  $850\,\pm\,60\,\mathrm{Pa}$ . We modeled the linear creep response of the fungal biofilm and found that *C. albicans* has a characteristic relaxation time of  $810\,\pm\,19\,\mathrm{s}$  and a viscosity of  $8.4\,\pm\,0.2\,\mathrm{MPa}\,\mathrm{s}$ . We applied this method to probe the effects of altered chitin deposition in the *C. albicans* cell wall. Differences between the biofilm's phenotypic cell shape and rheological properties in mutants with altered chitin synthase activity were resolved. Discovering how genotypic, phenotypic, and environmental factors impact the material properties of these microbial communities can have implications for understanding fungal biofilm growth and aid in the development of remediation strategies. © *2022 The Society* 

### I. INTRODUCTION

A biofilm is a community of microbial cells encased in an extracellular matrix and attached to a surface [1]. Biofilms can be formed by a variety of microbial life, including both bacterial and fungal species. Both bacterial and fungal biofilms are recognized as a major cause of infection and disease [2–4].

Biofilms—both bacterial and fungal—possess several common characteristics. In addition to the microbiological view of microbial cells encased in an extracellular polymeric substance (EPS) comprised of DNA, proteins, and polysaccharides, both bacterial and fungal biofilms have been explored as a class of soft matter. Biofilms are viscoelastic materials; the cells are rigid inclusions while the polysaccharide polymers in the EPS are either a complex fluid or gel [5]. These polysaccharides potentially interact with proteins and extracellular DNA also present in the EPS [6] as well as with the microbial cells themselves [7]. The resultant

The rheological properties of biofilms are of both fundamental and practical interest. Fundamentally, rheology is a measurement of phenotype that is sensitive to both genotype and environment. Technologically, biofilm rheology has implications for the understanding of microbial growth and its remediation. For example, exposing biofilms to shear forces, particularly fluid flow, impacts biofilm growth and structure. Biofilms grown under laminar or turbulent flow exhibit clustering and streamer formation [10,11]. Biofilms grown under high shear stress conditions (as characterized by the wall shear stress in channel flow) display more biomass as well as exhibit increased adhesion and cohesion [12]. Rheology has been used to probe the effects of chemical and antimicrobial agents [13] on mechanical properties. Biofilms (e.g., Pseudomonas aeruginosa) exhibit microstructure failure when exposed to high shear stress conditions [12]. Biofilms also show evidence of viscoelastic recoil [14]. Rheology can be correlated with genetic mutations and gene regulation; regulation of exopolysaccharide synthesis and export has been of particular interest [15]. Finally, cellular

viscoelasticity has been studied—primarily in bacterial biofilms—by both mechanical rheometry [8] and microrheology [9].

a) Author to whom correspondence should be addressed; electronic mail: mjsolo@umich.edu

morphology has been shown to impact the alignment and arrangement of bacterial cells during biofilm formation [16,17].

Thus, characterizing the mechanics and rheology of biofilms is increasingly common in microbiology, biomedical engineering, and environmental engineering. However, most methods and results to date concern bacterial biofilms. *Staphylococcus epidermidis* [8], *P. aeruginosa* [18], *Bacillus subtilis* [19], *Vibrio cholerae* [20], and *Klebsiella pneumoniae* [21] have been of particular interest. Biofilm rheology has been the subject of recent reviews [13,22–24]; these have focused almost exclusively on the structure and properties of bacterial biofilms. Rheological characterization of fungal biofilms could have utility similar to that of bacterial biofilms.

Fungi are a diverse kingdom of eukaryotic organisms capable of growing in single or multicellular forms. Single cellular forms of fungi are commonly referred to as yeasts, while multicellular forms are called molds or mushrooms, which produce filamentous hyphal cells [25]. Eukaryotic fungal cells are comprised of membrane-bound organelles, including nuclei that contain chromosomal DNA. Fungi have a cell wall containing glucans, chitin and chitosan, mannans and/or galactomannans, and glycoproteins [26]. Fungi are heterotrophs, acquiring nutrients from the environment, and can reproduce both sexually and asexually. Fungal cells are primarily immobile, except for spore dissemination used as a means of reproduction [25]. Many fungi are part of the human microbiome [27,28], but fungi can be found in other environments including in nature and industrial settings [29].

Fungi exhibit dimorphism, which is the ability to produce separated yeast-form and filamentous cells, such as hyphae or pseudohyphae, in a single species [30]. Yeast cells have an ovoidal shape. Hyphae are filamentous cells with a width of approximately  $2\,\mu m$  and parallel sidewalls. Pseudohyphae are an intermediate elongated cellular form with nonparallel sidewalls and a width greater than approximately  $2.8\,\mu m$  [31]. This classification has been systemized in the literature using aspect ratio as a characteristic measure. By this measure, yeast cells have an aspect ratio of < 1.5, pseudohyphae range from 1.5 to 2, and hyphae have an aspect ratio of > 2 [32]. For the purposes of this paper, yeast are referred to as ovoid-shaped, pseudohyphae are considered elongated ellipsoids, and hyphae are filaments.

Measuring the rheological properties of fungal biofilms presents some experimental challenges relative to their bacterial counterparts. For example, fungal biofilms take significantly longer to culture than bacterial biofilms. Bacterial biofilms adhere to a surface in about 5–120 min and are typically considered mature after 18 h of growth on the surface [33]. Fungal biofilms typically progress through three growth phases: the early phase, involving the adhesion of yeast cells to a surface, lasts up to 11 h; an intermediate biofilm establishment phase is characterized by cellular organization and the secreting of EPS requires 12-30 h; and a final maturation phase results in a three-dimensional (3D) biofilm structure that manifests after an additional 38-72 h [3]. This long establishment time makes in situ growth of the fungal biofilms on the rheometer—analogous to that performed by Pavlovsky et al. for bacterial biofilms—impractical because of the duration of rheometer usage required during this growth period.

An additional challenge to resolve is that fungal cells are eukaryotic and significantly larger  $(2-10\,\mu\text{m})$  than bacteria  $(0.2-2\,\mu\text{m})$ . The larger size complicates the application of microrheology techniques because the fungal cells are non-Brownian and, therefore, cannot themselves be used as *in situ* microrheology probes, like bacteria. Moreover, the cellular dimensions of fungal species are only a little more than an order of magnitude smaller than the typical fixture dimension of mechanical rheometry. Therefore, the effects of gap size on rheology might be anticipated.

Given these challenges, there have been very few studies investigating the rheology of fungal biofilms. However, such a rheological method could be broadly applied to research questions such as the influence of cell shape on rheological properties and the influence of antifungals or gene mutations on fungal biofilm viscoelasticity. Two studies of fungal biofilms that are available have characterized the elastic (G') and viscous (G") moduli in mixed-species biofilms comprised of the fungal species Rhodotorula mucilaginosa, Candida krusei, Candida kefyr, and Candida tropicalis [29,34]. These species are prevalent in the juice manufacturing industry. Both studies used a self-described ad hoc ring system to grow the biofilms under dynamic flow conditions typical of the juice manufacturing process. The ring was then attached to a rheometer for analysis. Brugnoni et al. demonstrated the viscoelastic nature of fungal biofilms and showed that G' was not affected by the flow conditions during growth. The mixed species biofilms had a reported critical yield strain between 1.5% and 5%, as calculated from a strain amplitude sweep [34]. Tarifa et al. explored how the food matrix, sugar concentration, and hydrodynamic conditions impacted biofilm rheological behavior. For all nutrient conditions, biofilms grown under turbulent flow had a higher modulus than those grown under quiescent conditions [29]. These papers represent a starting point for the exploration of fungal biofilm rheology. Additional work can address the measurement challenges identified earlier; correlation of such measurements with microstructural characterization of cell dimorphism would also be valuable.

The purpose of this paper is, therefore, to develop and characterize the performance of a method to characterize the rheological properties of fungal biofilms. The method developed addresses challenges that are characteristic of these complex materials. The method is validated for a range of fixture and measurement conditions. We then use the method to compare the viscoelastic properties of a series of chitin synthase mutants of *C. albicans*.

C. albicans was used as the model fungus in this study. C. albicans is an opportunistic pathogen. It is a member of the human microbiome and is known to cause infections such as candida vaginitis [27,35]. As described above with respect to many fungi, C. albicans exhibits polymorphism, with cells growing in one of three phenotypes: ovoid-shaped budding yeast, elongated ellipsoidal pseudohyphae, or true hyphae with parallel cell walls [36]. The morphological transition between yeast and filamentous pseudohyphal and hyphal forms is a primary virulence factor along with the

TABLE I. C. albicans chitin synthase classes and functions.

Chitin synthase	Class	Functions
Chs1	Class II	Chitin synthesis at the primary septum; contributes to the general structural integrity of the cell wall; essential for cell viability
Chs2, 8	Class I	In vitro chitin synthase activity observed; chitin deposition at polarized tips of hyphae and cells and at sites of septation
Chs3	Class IV	Principal synthase for chitin deposition in the cell wall; chitin deposition in the chitin ring at division sites

formation of adhesins and invasins on the cell surface, and the secretion of hydrolytic enzymes [27].

Cell wall function is critical in the C. albicans life cycle, providing cell structural integrity as well as a platform for cell-cell and cell-substrate interactions [37]. Chitin is a major component of the fungal cell wall. Chitin is a linear polysaccharide of  $\beta$ -(1,4)-linked N-acetylglucosamine capable of hydrogen bonding [26,38]. Chitin makes up between 1% and 15% of the cell wall mass. The yeast cell form possesses 1-2% chitin, while hyphae have 15% chitin [26]. In C. albicans, chitin is synthesized by four chitin synthase enzymes belonging to three functional classes (Table I). The chitin synthase enzyme classes differ in their protein structure and functionality. The respective chitin synthase activities are spatially restricted and function predominantly to promote cell wall structure in the lateral cell, at sites of highly polarized growth, and/or at the primary septum, or neck, between dividing cells [Fig. 1(a)]. Chitin synthase activity is required for wild-type cell wall function, but the effect of these enzymes on the viscoelastic properties of fungal biofilms is unclear. We hypothesized that altered chitin synthase activity would affect the rheology of C. albicans biofilms [Fig. 1(c)]. To test this, we generated deletion mutants of chitin synthase genes from each of the three enzyme classes and applied our method to determine the rheology of biofilms in the *C. albicans* mutants.

For this study, we first describe a method to culture fungal biofilms in specimens that can be used in parallel plate rheometry. We then report the viscoelastic properties of *C. albicans* wild-type biofilms as characterized by oscillatory shear and creep rheology. We conclude by measuring the rheology of biofilms of several chitin synthase mutants, thereby evaluating the effect of chitin on fungal biofilm mechanics. The rheological measurements are contextualized

using a set of morphological measurements collected at different scales by means of stereoscopic and confocal microscopy.

#### II. METHODS

## A. Fungal strains and growth conditions

C. albicans BWP17 is isogenic to laboratory strain SC5314 [39] (ATCC) and stored at -80 °C as a glycerol stock. BWP17 (ura3::imm434/ura3::imm434 iro1/iro1:: imm434 his1::hisG/his1::hisG arg4/arg4) is a widely used laboratory strain with convenient auxotrophies suitable for genetic manipulation. The fungi were streaked onto yeast extract peptone dextrose (YPD) agar and incubated at 30 °C for 2 days. A single colony was used to inoculate 10 ml of YPD broth medium and cultured overnight in preparation for biofilm growth described below. Heterozygous and homozygous deletion mutants in C. albicans were generated according to standard protocols by allele replacement [40,41]. By convention, wild-type C. albicans gene names are italicized in capital letters, while mutants are italicized in lower case. The names of C. albicans proteins are not italicized and are presented with the first letter capitalized.

## B. Biofilm growth for rheology

The requirements for culture are that the biofilm is a cohesive, homogeneous material of dimension suitable for parallel plate rheometry (the plate diameter used in this study is 8 mm). The strategy is to grow the fungal biofilm within a mold of diameter slightly greater than the dimension of the parallel plate fixture. There is no standard protocol to grow fungal biofilms in this way; however, the literature indicates that typical methods of growth involve coating a solid substrate with an adhesive agent such as fetal bovine serum (FBS) before inoculating the surface with overnight fungal culture and allowing biofilms to develop during a period that varies between 6 h and 11 weeks, depending on the growth rate of the fungal strain and biomass requirements of the study [34,42,43]. In the present case, a growth period of 2 weeks was required.

Briefly, a 47 mm polycarbonate membrane, pore size 1 μm (Cytiva Whatmam, Marlborough, MA) was placed on an agar plate with Spider medium. The Spider medium included the following: 5 g of Difco Nutrient broth (Becton, Dickinson and Company, Sparks, MD), 1 g K<sub>2</sub>HPO<sub>4</sub> (Fisher BioReagents, Waltham, MA), 5 g mannitol (Fisher Scientific, Fair Lawn, NJ), 40 mg Uridine (Acros Organics, Fair Lawn, NJ), and 7.5 g agar (Acros Organics, Fair Lawn, NJ) per 500 ml of media. Each membrane had two, 25.4 mm (10.3 mm inner diameter) polyether ether ketone (PEEK)

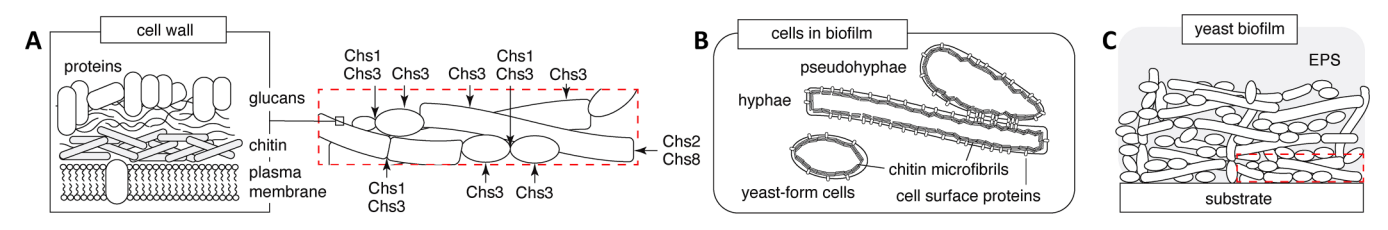


FIG. 1. Chitin is a major component of the fungal cell wall and its distribution is controlled by four chitin synthase classes at specific locations within the cell (a). Fungal cells exist in one of three cellular forms (b) and are suspended in a matrix of EPS, capable of adhering to a substrate (c).

washers (W.W. Granger Inc., Lake Forest, IL) placed on top. Then, 200 µl *C. albicans* overnight culture was added to each washer and the covered plate was incubated at 30 °C for 1 week. After 1 week, the filter/washer assembly was sterilely transferred to a fresh Spider agar plate and returned to the 30 °C incubator for an additional week. Figure 2(a) shows the mature biofilm in the washer assembly after 2 weeks of growth.

Rheological measurements were performed on a TA DHR-3 Rheometer (TA-instruments, New Castle, DE). Self-adhesive 600 grit sandpaper was adhered to both the Peltier plate and the 8 mm flat plate rheometer geometry [44,45]. Additional measurements performed for 400 grit sandpaper demonstrated comparable results (cf. Fig. S1 in the supplementary material) [55]. The rheometer gap was zeroed, and the instrument was calibrated for system inertia, with the sandpaper surfaces attached. The temperature was held constant at 25 °C. After 2 weeks of growth, the biofilm was a solid, cohesive material that could be transferred as a wafer onto the bottom plate of the rheometer. The handling and loading of the mature biofilm were similar to that of glassy polymer melts [e.g., Poly(dimethylsiloxane) (PDMS)], thermoplastics [e.g., poly(methyl methacrylate) (PMMA) and Acrylonitrile butadiene styrene (ABS)], or foams (e.g., neoprene). After placement on the bottom geometry, the specimen was cut out of the biofilm by means of an 8 mm biopsy punch (Integra Miltex, Princeton, NJ) as shown in Fig. 2(b). The geometry was partially lowered to a gap of 2000 µm, the sample aligned using a spatula and tweezers [Fig. 2(c)], and SF96-350 silicone oil (GE Silicones, Boston, MA) was applied around the exposed edges. The geometry was then lowered until an axial force of 0.1N was registered [Fig. 2(d)] [19]. Given the fixture geometry, this corresponds to a normal stress of 2000 Pa. The sample, thus, filled the gap completely, and this gap dimension varied from 500 to  $1100\,\mu m$ , depending on the specimen. This range is a consequence of the normal variability of fungal growth over 2 weeks; determining the gap by the normal stress controlled for these differences.

## C. Rheological measurements

Rheological measurements were performed in both strainand stress-controlled modes. The small- and large-amplitude oscillatory measurements were performed in the former mode, and the creep measurements in the latter. For the oscillatory rheological measurements, after sample loading, the specimen was rested for t = 60 s. The linear viscoelastic moduli G' and G" were measured using small-amplitude oscillatory deformation. The strain amplitude for linear measurements was selected to be  $\gamma_0 = 0.0008$  as per the results of preliminary strain sweep measurements. The frequency range was  $\omega = 0.1 - 10 \, \text{rad s}^{-1}$ . Oscillatory strain sweeps were then performed over  $\gamma_0 = 0.01 - 200$  at  $\omega = 1 \,\mathrm{rad}\,\mathrm{s}^{-1}$ . The fixture was an 8 mm flat plate with 600 grit self-adhesive sandpaper applied. For the initial wild-type measurements, frequency and strain sweeps were performed in series to minimize sample preparation. When evaluating the mutant strains,  $chs3\Delta$  and  $chs8\Delta/\Delta$  exhibited signs of strain conditioning when running frequency and strain sweeps in series. Here, by straining conditioning, we refer to very slight but resolvable changes in measured rheological properties upon sustained small-amplitude deformation, likely generated by an accumulation of small, deformation-induced structural changes. Subsequently, each measurement during mutant evaluation was performed on an individual sample.

Creep rheology measurements were performed in the following way: The creep compliance  $J(t, \sigma_o)$  was measured to

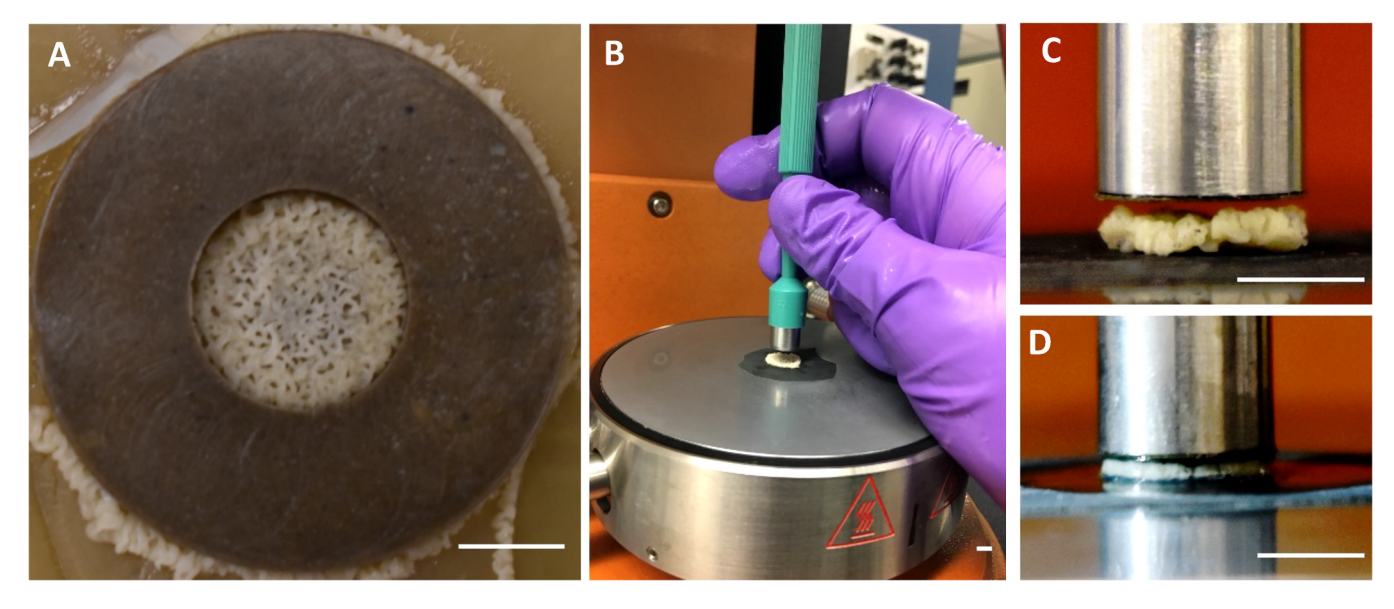


FIG. 2. The fungal biofilm material at critical steps in the rheological testing procedure. (a) *C. albicans* biofilm grown in a sterile PEEK ring on a spider agar plate for 2 weeks. (b) The entire biofilm is transferred to the sandpaper lined Peltier plate of the rheometer. A 8 mm biopsy punch is used to cut the sample to the same size as the parallel plate fixture. (c) The rheometer geometry is lowered to a gap height of 2000 μm and the sample is aligned with the top geometry to ensure the entire gap is filled. (d) After alignment, the geometry is lowered until an axial force of 0.1 N is achieved. This results in a specimen-dependent gap height due to the variations in thickness of the cultured biofilm; when lowered to an axial force of 0.1 N, the top geometry has complete contact with the sample. The gap in (d) is 960 μm. Silicone oil has been applied to the edges of the sample. All scale bars are 5 mm.

determine the nonlinear rheological response of the fungal biofilms and determine the yield stress. These measurements were performed for 30 min at the following magnitudes of the applied stresses: 700, 800, 900, and 1000 Pa. For each applied stress, the strain deformation,  $\gamma$ , was recorded as a function of time and plotted as the creep compliance  $J(t, \sigma_o) = \gamma(t)/\sigma_o$ . At low applied stress, the compliance reaches a plateau value at intermediate times. However, at high applied stress, the compliance steadily rises, approaching a near linear increase with time at long times. The stress of the transition between these two regimes of behavior is an indicator of the specimen's yield stress. These stresses were selected to range from within the linear region to above the yield stress.

# D. Stereoscopic imaging of fungal biofilm specimens used for rheometry

Stereoscopic images of fungal biofilm samples were taken using a Motic SMZ-171 microscope fitted with a Moticam 33.0MP camera. The magnification was  $7.5 \times -50 \times$  and the field of view encompassed the entire specimen.

# E. Confocal laser scanning microscopy of fungal biofilms

Stained biofilms were imaged using a Nikon A1RSi confocal laser scanning microscope, equipped with a CFI Plan Apo Lambda  $100\times$  oil lens objective with a numerical aperture (NA) of 1.45. The culture method for confocal microscopy imaging was the following:  $250\,\mu l$  of fungal overnight culture was added to  $500\,\mu l$  spider media in a Nunc Lab-Tek II chambered cover glass dish (Thermo Fisher Scientific). The chamber was sealed with parafilm to prevent desiccation and placed on a shaker for 24 h at 50 rpm. The sample was stained with  $1\,\mu l$  FUN-1 Cell Stain (ThermoFisher) and  $1\,\mu l$  Calcofluor White Stain (Sigma-Aldrich) and then returned to a 50-rpm shaker for 5 min.

FUN-1 is a two-color (green/red) fluorescent probe for yeast and fungal viability. It passively diffuses into the cells and initially stains the cytoplasm green. In metabolically active cells, intravacuolar structures will become stained with an accompanying fluorescence shift to red after an extended period. In this study, FUN-1 was used solely as a cytoplasm stain; the metabolic fluorescence shift was observed but not quantified or reported. The excitation wavelength of FUN-1 is 480 nm, fluorescein isothiocyanate (FITC) filters captured the green cytoplasm emission spectra of 490–525 nm, and Texas Red filters captured the red intravacuolar structure spectra over 570–620 nm. Calcofluor White is a nonspecific stain that binds to chitin and cellulose in the cell walls of fungi. It has an excitation wavelength of 355 nm and an emission spectral range of 423–443 nm.

To ensure representative sampling of the biofilm, five images were captured at points in the specimen corresponding to the shape of a cross. This cross was centered on the chamber. This procedure was repeated three times for a total of 15 images analyzed for each mutant. Each frame was  $512 \times 512$  pixels (px) (124.24 nm/px) and taken  $500 \, \mu m$  apart. Imaging was performed at a distance  $10 \, \mu m$  above the coverslip.

Image analysis was performed to determine the number of each of the cell shape phenotypes (i.e., yeast, pseudohyphae, and hyphae) present in each of the images. Single frame RGB images of the cells dyed with FUN-1 cytoplasm stain were loaded into MATLAB. MATLAB's two-dimensional (2D) canny edge detection feature was used to outline each of the cells and fill inside of the cell so that all cells were converted into individual white regions. These images were then converted into 8-bit, black and white images and loaded into a custom python code utilizing tools from the open-source python algorithms collection scikit-image. The label image region and measure region properties' commands were used to measure the length and width of each cell. These measurements were then converted to aspect ratio by dividing the longer dimension by the shorter dimension. The output of the image analysis was the aspect ratio of each cell in the  $63 \times 63 \,\mu\text{m}^2$  field of view.

#### III. RESULTS

## A. Fungal biofilm morphology

The biofilm initially grows as a single layer of confluent cells, completely covering the agar substrate on which it sits. After approximately 1 week of growth, the biofilm begins to grow perpendicular to the surface; fused strands also begin to develop randomly. Figures 3(a) and 3(b) show a mature wildtype biofilm after 2 weeks of growth. It is a complex network of entangled strands, each of diameter about 200-500 µm. As visible in Fig. 3(a), top view—that is, viewing the surface of the biofilm exposed to air during growth—the biofilm folds create voids. These voids are present throughout the specimen; however, their size and distribution are heterogeneous, varying from about 50 to 300 µm in its shortest dimension and as great as 800 µm on its longest dimension. When the sample is viewed from the bottom—that is, the surface of the biofilm adhered to the agar nutrient plate during growth—as shown in Fig. 3(b), the fungal biofilm is confluent and void-free. Thus, the morphology of the biofilm varies in the z-direction. Visual inspection of Figs. 3(a) and 3(b) indicates that the morphology is uniform in a plane parallel to the substrate. Images of the yielded biofilm material can be found in Fig. S2 in the supplementary material [55].

On the microscopic scale, cellular homogeneity is observed. Figures 3(c) and 3(d) show 3D confocal images of a mature wild-type biofilm. The biofilm is comprised of cells of various sizes and shapes with no apparent alignment or arrangement. In these images, blue is Calcofluor White staining the cell wall and green/red is the FUN-1 cytoplasm stain. Figure 3(c) has a voxel size of  $0.248 \times 0.248 \times 0.248 \, \mu m^3$ , and Fig. 3(d) has a voxel size of  $0.124 \times 0.124 \times 0.124 \, \mu m^3$ . Figure 3(e) is a 2D slice of Fig. 3(d) obtained 2.88  $\mu$ m above the sample coverslip for visualization on a cellular level.

## **B.** Method evaluation

Three factors that impact mechanical rheometry measurements were explored to determine the degree to which they impact biofilm rheological measurements: the rheometer gap, the evaporation barrier coating, and the sample diameter.

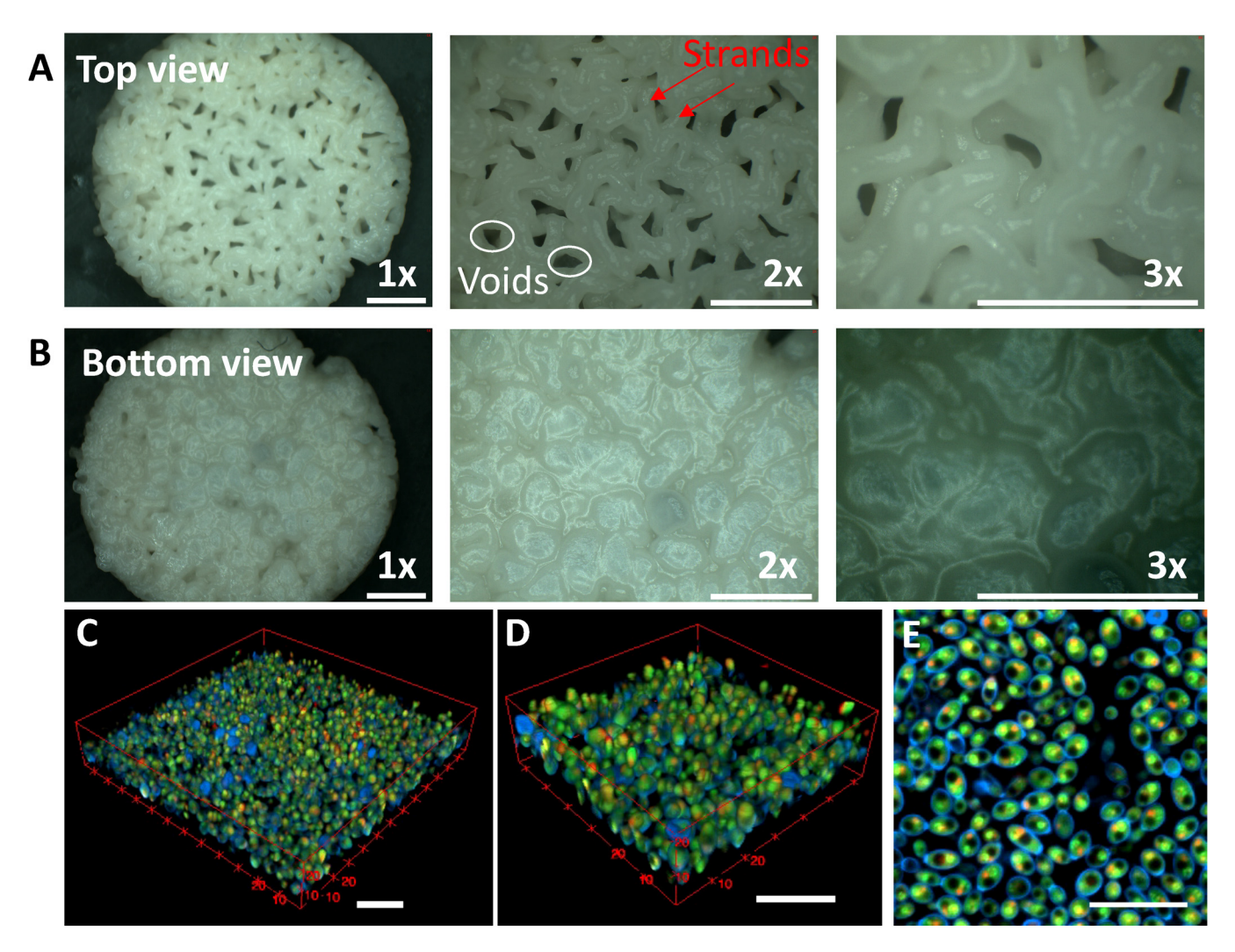


**FIG. 3.** Stereoscope images of wild-type *C. albicans* biofilm after 2 weeks of growth [(a) and (b)] prior to rheological testing. The same sample is shown at  $1 \times 2 \times$ , and  $3 \times 200$  and  $3 \times 200$ 

The culture method generates natural variation in the height of the biofilm specimens. To study this variability, 20 different cultures were tested. Frequency-dependent linear viscoelastic moduli are reported in Fig. 4(a), and the effect of strain amplitude is reported in Fig. 4(b). The rheometer gap in each instance is established by compressing the specimen until the normal stress is 2000 Pa.

Under these conditions, the specimen gap heights (h) ranged from 500 to 1100  $\mu$ m. To analyze the dependence of the rheological measurements on gap dimension, the data were grouped into three bins. The groupings were such that the range of each bin is approximately 200  $\mu$ m;  $500 \,\mu$ m  $\leq h_1 < 700 \,\mu$ m,  $700 \,\mu$ m  $\leq h_2 < 900 \,\mu$ m, and  $900 \,\mu$ m  $\leq h_3 < 1100 \,\mu$ m with sample number (N) in each bin:  $N_1 = 5, N_2 = 9$ , and  $N_3 = 6$ . There were no statistical differences between the G' for any gap height. This indicates that the measurements were conducted at gaps large enough to avoid gap effects.

Fungal biofilms are hydrated materials that experience drying due to solvent evaporation if exposed to ambient air for long lengths of time. Indeed, at  $\gamma_0 = 0.08$ ,  $\omega = 1$  rad/s,

the linear elastic modulus, G', varies significantly over the period of 1 h (Fig. S3 in the supplementary material) [55]. Significant evaporation, thus, occurs during the rheological measurement. To minimize evaporation, silicone oil was applied to the outer edge of the sample after it was loaded onto the rheometer. Silicone oils of three different kinematic viscosities—3.5, 10, and 100 cm<sup>2</sup>/s—were evaluated. The results [Figs. 5(a) and 5(b)] showed that the silicone oil kinematic viscosity had no impact on the biofilm rheological properties and that the time-dependent effects observed in Fig. S3 in the supplementary material [55] were eliminated. The 3.5 cm<sup>2</sup>/s silicone oil was used in all subsequent experiments. Although silicone oil is inert and commonly used to prevent evaporation in rheology, tests were performed to determine if the oil would affect the living biofilms studied here. Tests were performed under the following protocol: the sample was loaded, and the silicone oil applied. After a 45 min waiting period, a time selected to be greater than the duration of any experiment reported in this paper,  $G'(\omega)$  and  $G''(\omega)$  were measured at  $\gamma_0 = 0.08$  [Fig. 5(c)], and a strain amplitude sweep performed at  $\omega = 1$  rad/s [Fig. 5(d)]. As

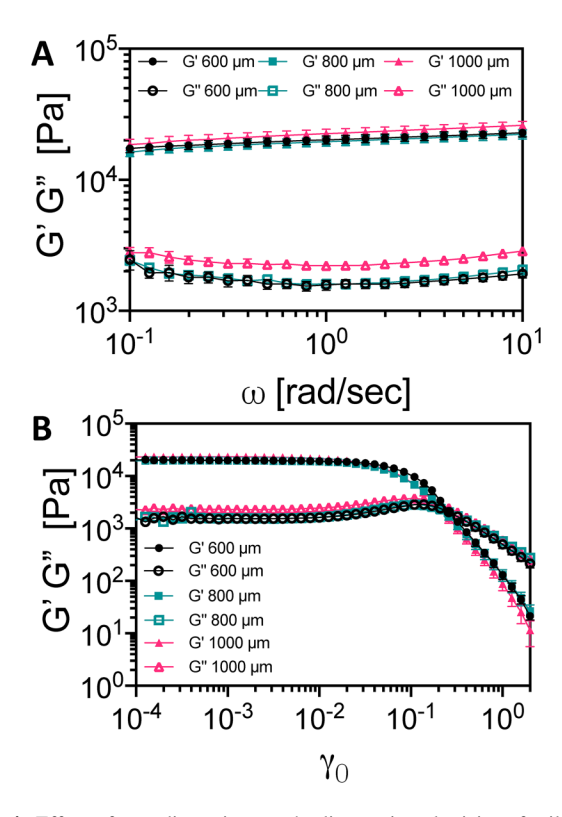


**FIG. 4.** Effect of gap dimension on the linear viscoelasticity of wild-type *C. albicans* biofilm at gaps of  $h = 600 \pm 100$ ,  $800 \pm 100$ , and  $1000 \pm 100 \,\mu\text{m}$ . Storage and loss moduli (G', G") as a function of (a) frequency at  $\gamma = 0.08$  and (b) strain amplitude at  $\omega = 1 \,\text{rad/s}$ . Error bars are standard error of the mean.

demonstrated in Figs. 5(c) and 5(d), there were no differences in measurements performed with or without this waiting period. The congruence indicates that the silicone oil did not affect the material properties of the biofilm over the maximum duration of any measurement in this study.

As shown in Fig. 3, the fungal biofilm structure contains strands and voids of various sizes. To study if these relatively large structures could impact the measurements, a smaller diameter, 6 mm sample was tested and compared to the 8 mm sample used to match the fixture size. Figure 6 is a comparison of G' and G" with respect to frequency [Fig. 6(a)] and strain [Fig. 6(b)]. There is no apparent difference in the modulus of the 6 and 8 mm samples.

## C. Fungal biofilm rheological characterization

Small-amplitude oscillatory rheology was used to determine the linear viscoelastic moduli of wild-type C. albicans as a function of [Fig. 7(a)] frequency and [Fig. 7(b)] time. The elastic modulus G' and the viscous modulus G'' were nearly independent of frequency, with an average magnitude of  $18\,400\,\pm\,1100\,\mathrm{Pa}$  and  $1700\,\pm\,140\,\mathrm{Pa}$ , respectively, at a frequency of 1 rad/s.

The frequency dependence [Fig. 7(a)] of the linear viscoelastic moduli shows that G' is greater than G" by approximately a factor of 10. Both G' and G" are approximately independent of frequency with the average  $\tan \delta = 0.10 \pm 0.01$  across all frequencies. This is characteristic of a gel-like, viscoelastic material in the rubbery plateau region.

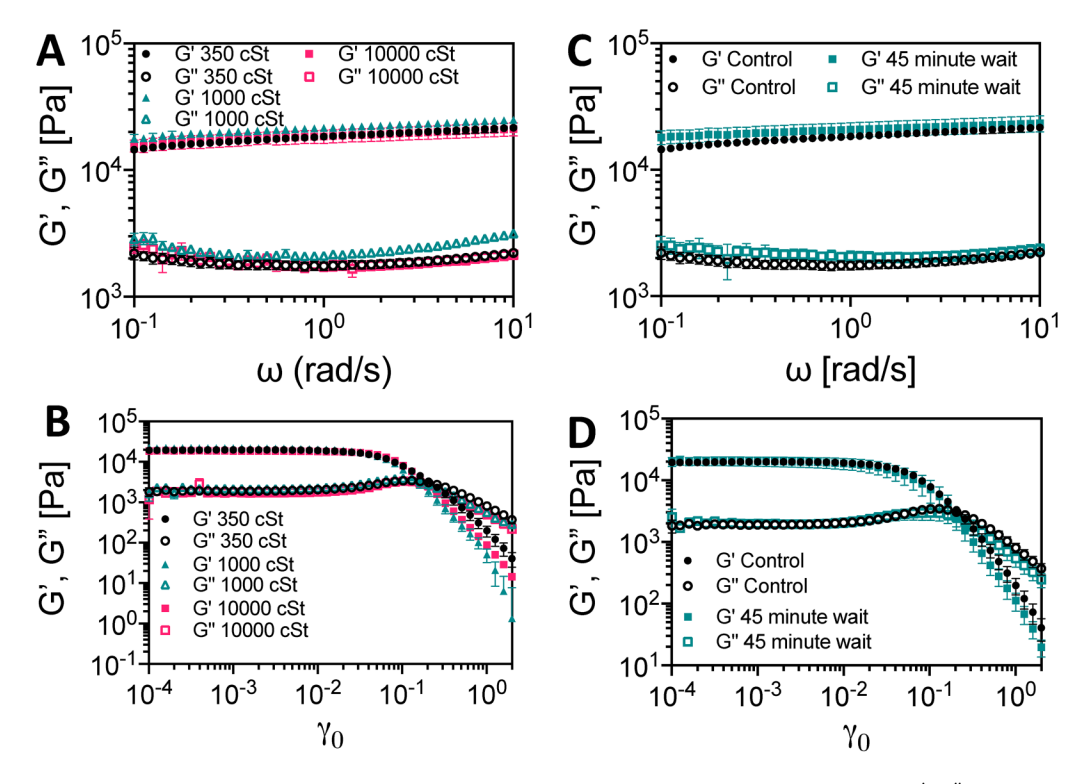


**FIG. 5.** Effects of evaporation and the use of silicone oil on sample during rheological testing. Storage and loss moduli (G', G'') as a function of (a) frequency at  $\gamma_0 = 0.08$  and (b) strain amplitude at  $\omega = 1$  rad/s using three silicone oils of kinematic viscosities 350, 1000, and 10 000 cSt. Storage and loss moduli (G', G'') as a function of (c) frequency at  $\gamma_0 = 0.08$  and (d) strain amplitude at  $\omega = 1$  rad/s performed with and without a 45 min waiting period after the sample was loaded onto the rheometer, silicone oil applied, and geometry lowered. Error bars are standard error of the mean.

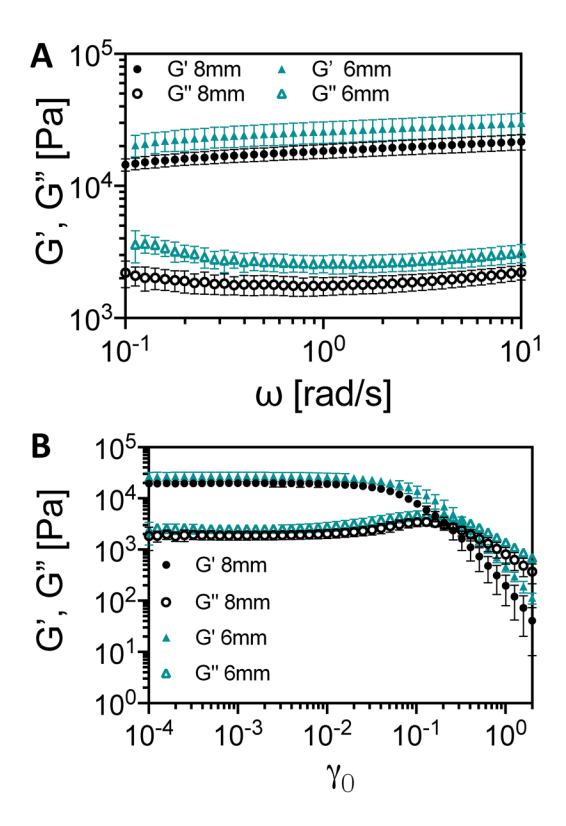


**FIG. 6.** Effects of sample diameter on rheological properties. Storage and loss moduli (G', G'') as a function of (a) frequency at  $\gamma_0 = 0.08$  and (b) strain amplitude at  $\omega = 1$  rad/s. Error bars are standard error of the mean.

Furthermore, Fig. 7(b) shows that the fungal biofilm linear rheological properties are nearly time-independent for  $t > 200 \,\mathrm{s}$ .

The strain amplitude sweep [Fig. 8(a)] of the wild-type fungal biofilm shows an onset of nonlinearity at a strain of 0.0145. The onset of nonlinearity is here taken as a 5% deviation of G' from its value of  $19\,600\pm240\,\mathrm{Pa}$  in the linear regime. The strain chosen for the frequency and time sweeps [Figs. 7(a) and 7(b), respectively] was  $\gamma_0 = 0.0008$ , which is within the linear regime. The critical yield strain, defined by the intersection of G' and G," is  $\gamma_y = 0.23\pm0.04$ . An overshoot—that is, an increase in modulus relative to the linear plateau prior to yielding—in G" of about 50% over the plateau value of 1900 Pa is observed prior to the critical

yield strain. This is characteristic of weak strain overshoot and could suggest macromolecules are aligning and resisting deformation prior to yielding, consistent with other yielding and transient network materials [46].

The oscillatory strain amplitude data can be used to determine the yield stress of a viscoelastic material as the maximum value of elastic stress [47,48]. The elastic stress—the product  $G'\gamma_0$ —is plotted in Fig. 8(b). This treatment finds the yield stress to be 850  $\pm$  60 Pa.

The time-dependent creep compliance was measured at several values of the applied stress to study the nonlinear rheology of *C. albicans* biofilms (Fig. 9). Three replicates were measured at five applied stresses: 700, 800, 850, 900, and 1000 Pa. For each measurement, the sample may yield or remain intact. Figure 9(a) displays data for the applied stresses of 700 and 800 Pa where none of the three replicates yielded, and 1000 Pa where all three samples yielded. Figures 9(b) and 9(c) display the individual replicate data for 850 and 900 Pa, respectively. At 850 Pa, one sample yielded while two samples remained intact, while at 900 Pa, two samples yielded, and one sample remained intact. This behavior is likely a consequence of the biological variability of the fungal biofilm specimens.

At low applied stress-700 and 800 Pa-the biofilm exhibits behavior consistent with a viscoelastic solid with long-term creep. There is a near-instantaneous step response in compliance, followed by a plateau region, and then a small, progressive increase in compliance at long times. At high applied stress-1000 Pa-the creep compliance is nearly linear as a function of time. This response is characteristic of a viscoelastic liquid. The transition between solidlike and liquidlike behavior occurs around an applied stress of 850-900 Pa. We, therefore, assign a yield stress of 875 Pa. After the initial step response, the yielded samples have an upturn, which indicates a transition from solidlike deformation to liquidlike flow, while the test at 800 Pa does not flow. These data are in good agreement with the yield stress found from the elastic stress curve, which was  $850 \pm 60 \,\mathrm{Pa}$ . At applied stresses where the sample yielded, the specimen fragmented and was expelled from the gap.

A simple model of a viscoelastic solid was used to characterize the creep compliance in the low stress limit. The creep response of *C. albicans* is functionally similar to previous

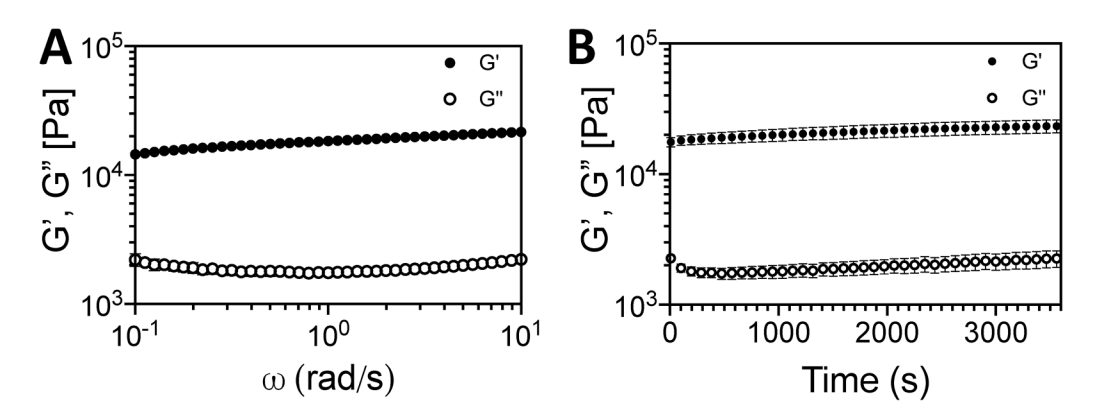


**FIG. 7.** Frequency and time sweep. Storage and loss moduli (G', G'') of wild-type *C. albicans* as a function of (a) frequency  $\omega$  at  $\gamma_0 = 0.0008$  and (b) time at  $\gamma_0 = 0.0008$ ,  $\omega = 1$  rad/s. These data include the average of four replicates. Error bars are standard error of the mean.

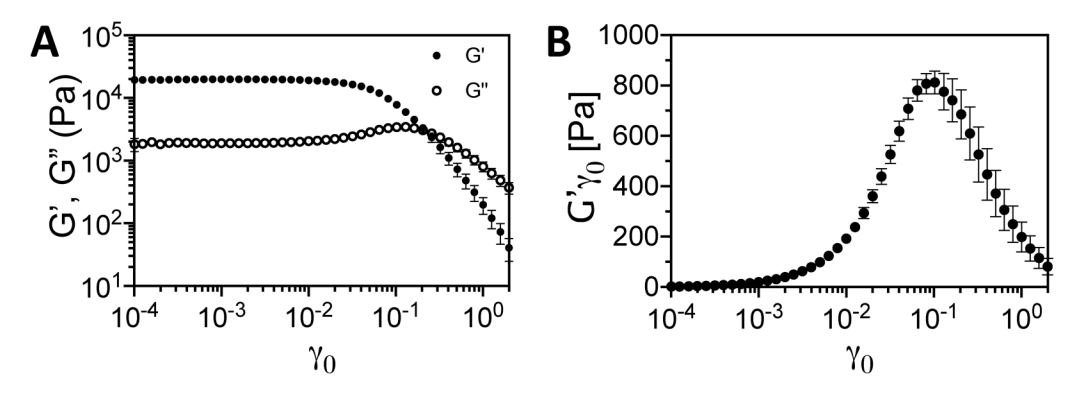


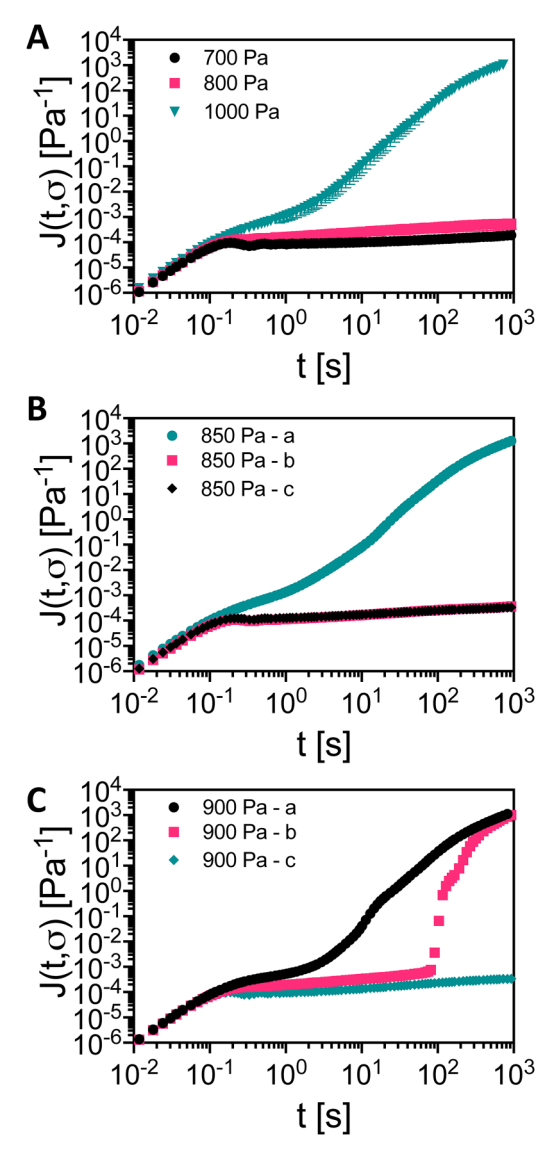
**FIG. 8.** Strain sweep and elastic stress. (a) Strain amplitude sweeps at  $\omega = 1$  rad/s for *C. albicans* biofilms. (b) Elastic stress  $(G'\gamma_0)$  plotted as a function of strain amplitude. The intersection point and the maximum of the curve are taken to be the yield stress in each graph, respectively.

reports for bacterial biofilms. That is, the rapid attainment of an elastic plateau is followed by a regime of viscous creep at long times. In previous work, Burgers, Kelvin–Voigt, and Jeffreys models were used to model such a response in bacterial biofilms [8,49]. We fit the *C. albicans* fungal biofilm creep data to the Jeffreys model, which captured both the rapid elastic plateau and the long-time creep response. The Jeffreys model, its equations, and parameter fits are reported in Table II. (The Kelvin–Voigt model was also considered; however, it did not capture the long-time creep. The Kelvin–Voigt model produced an elastic modulus  $G_1$  approximately 11% different than computed by the Jeffreys model.)

The Jeffreys model incorporates an elastic modulus  $(G_1)$ , a short-time viscosity  $(\eta_1)$ , a long-time creep viscosity  $(\eta_2)$ , and an inertial term (I). (We note that the inertial term in the model description addresses the coupling between the viscoelasticity of the material and the mass of the rheometer tooling that executes the deformation.) As apparent in Fig. 10, the model fit agrees very well with the experimental data.  $\eta_1$  is optimized for the best overall fit at the expense of capturing the magnitude of the ringing apparent at short times. The viscous terms were found to be  $860 + 30 \,\mathrm{Pa}\,\mathrm{s}$ and 8.4  $\pm$  0.2 MPa s for  $\eta_1$  and  $\eta_2$ , respectively. The modulus was found to be 10 300 Pa. The relaxation times of the biofilm are both  $810 \pm 19 \,\mathrm{s}$  Relaxation times are calculated as follows:  $\lambda_1 = (\eta_1 + \eta_2)/G_1$  and  $\lambda_2 = \eta_2/G_1$ . The long relaxation time observed is consistent with the transition from solid to viscous behavior observed at very long times in Fig. 10. We note that the rest time prior to initiating measurements in this paper is 60 s and it is useful to consider this rest time in light of the Fig. 10 results. After a rest period of 60 s, Fig. 10 indicates that the specimen is in the elastic plateau. That is, the material has elastically complied with the imposed stress, but has not had the opportunity to undergo significant viscous flow in response to this stress.

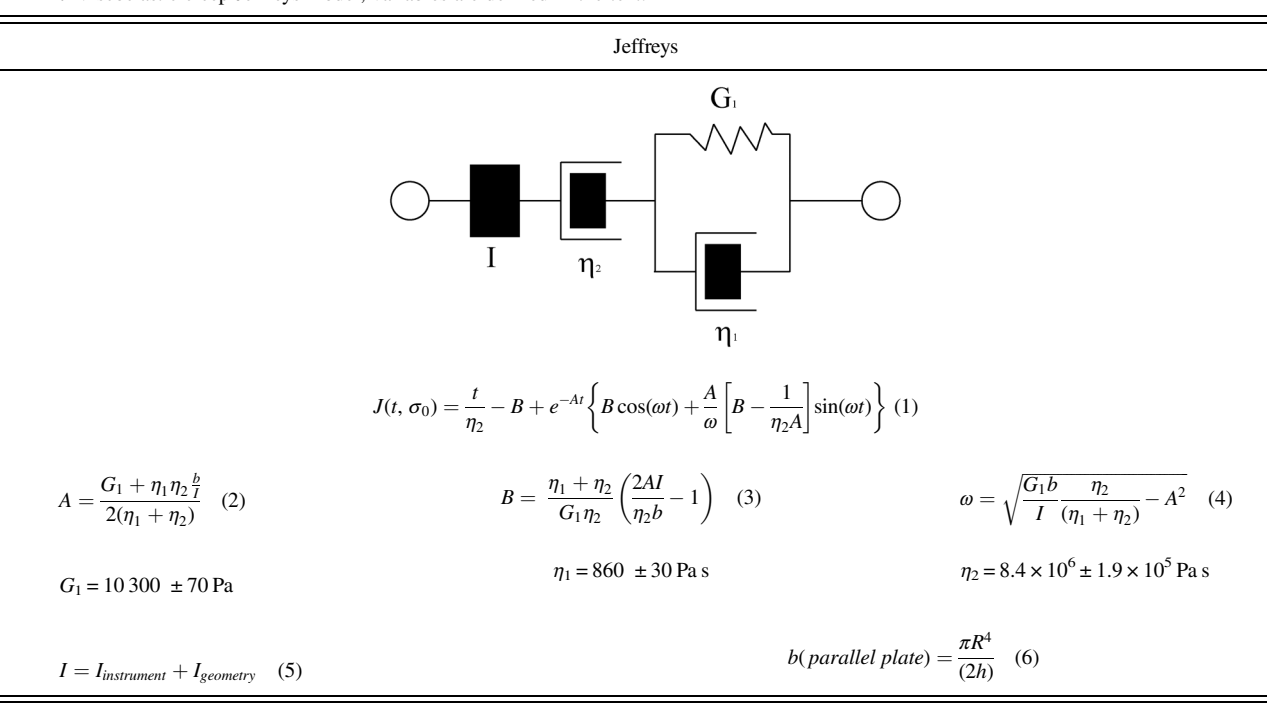
## D. Material structure of chitin-synthase mutants

With this method in place for the measurement of fungal biofilm rheology, we sought to test our hypothesis that chitin synthase activity affects the viscoelastic properties of C. albicans biofilms. In conjunction with rheological measurements, observations of the morphologies of wild-type and  $chs1\Delta/CHS1$ ,  $chs3\Delta/CHS3$ , and  $chs8\Delta/\Delta$  deletion mutants



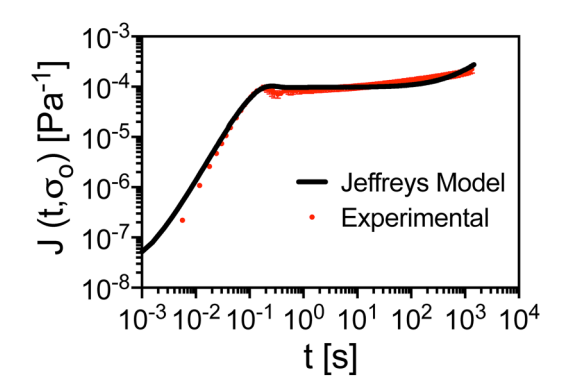
**FIG. 9.** Creep compliance  $J(t,\sigma)$  of wild-type *C. albicans*. A constant stress was applied at t=0 and the material compliance was measured over 30 min. (a) The average of three replicates for creep testing at a constant stress of 700, 800, and 1000 Pa. None of the sample yielded at 700 or 800 Pa, while all three samples yielded under 1000. Error bars are standard error of the mean. (b) Three repeated measures [(a)-(c)] of creep compliance at 850 Pa. One sample yielded, while two did not. (c) Three repeated measures [(a)-(c)] of creep compliance at 900 Pa. Two samples yielded, while one did not.

TABLE II. Viscoelastic creep Jeffreys model; variables are defined in the text.



were recorded by confocal microscopy. Figures 11 and 12 outline these qualitative and quantitative differences, respectively. Figure 11(a) are images of the biofilms prior to rheological testing as acquired by stereoscopy. Qualitatively, biofilms formed by the wild type,  $chs1\Delta$ , and  $chs3\Delta$  strains were very similar. The biofilms grew to the edge of the PEEK ring, filling the entire growth surface. When removed, these three strains were robust and could easily be transferred to the rheometer stage. The  $chs8\Delta/\Delta$  deletion mutant, however, was qualitatively different from the three other strains. Samples from  $chs8\Delta/\Delta$  did not fill the entire growth surface, leaving rough edges and gaps at the edges of the PEEK ring. The  $chs8\Delta/\Delta$  biofilms appeared more brittle than the other three strains; care was taken when transferring them onto the rheometer. The submillimeter strands and voids described in Fig. 4 are also apparent in these mutant strains.

Figures 11(b) and 11(c) are confocal micrographs of biofilms from the wild-type and chitin synthase mutant strains for field of views of  $127 \times 127 \text{ sq} \, \mu\text{m}$  and  $63 \times 63 \text{ sq} \, \mu\text{m}$ ,



**FIG. 10.** Jeffreys model. Linear region of creep of *C. albicans* (stress of 700 Pa) fit with the Jeffreys model. Error bars are standard deviation.

respectively. The biofilms appear to have cells of various sizes and shapes uniformly distributed among the samples. Examples of yeast-form cells, pseudohyphae, and hyphae are identified in Fig. 11(c) by circles, triangles, and rectangles, respectively. Biofilms from the wild-type,  $chs1\Delta$ , and  $chs3\Delta$  strains exhibit a similar distribution of cells, while biofilm from the  $chs8\Delta/\Delta$  deletion mutant contains more elongated cells that are characteristic of hyphae and pseudohyphae. These cells are more clustered than cells from the other mutants.

The respective distribution of yeast-form cells, pseudohyphae, and hyphae in biofilms from the strains tested is quantified in Fig. 12, as per Sec. II. Three  $\chi^2$  tests were performed, comparing the frequency of each cell type for each mutant to the expected wild-type distribution. There is no statistical difference between the wild-type cell counts and the cell counts for the  $chs1\Delta$  mutant. As indicated in Fig. 12(a), there is a statistical difference in the distribution of cells when comparing biofilms from wild type to chs3 $\Delta$  (P = 0.0055) and wild type to  $chs8\Delta/\Delta$  (P < 0.0001). Although biofilms from the wild-type,  $chs1\Delta$ , and  $chs3\Delta$  strains appear to have a larger fraction of yeast cells than biofilms from  $chs8\Delta/\Delta$ , and  $chs8\Delta/\Delta$  biofilms appear to have the largest fraction of hyphae, a two-way ANOVA analysis with multiple comparisons on the cell fractions [Fig. 12(b)] shows no significant difference of the aspect ratio distributions. From the data in total, we do observe differences in the cell type composition of biofilms from chitin synthase mutants relative to wild type.

## E. Rheology of chitin synthase mutants

Small-amplitude oscillatory rheology was performed for the wild-type and three chitin synthase mutant strains of C. albicans. Figure 13 shows G' and G'' as a function of frequency at  $\gamma_0=0.0001$  [Fig. 13(a)], and strain at  $\omega=1$  rad/s

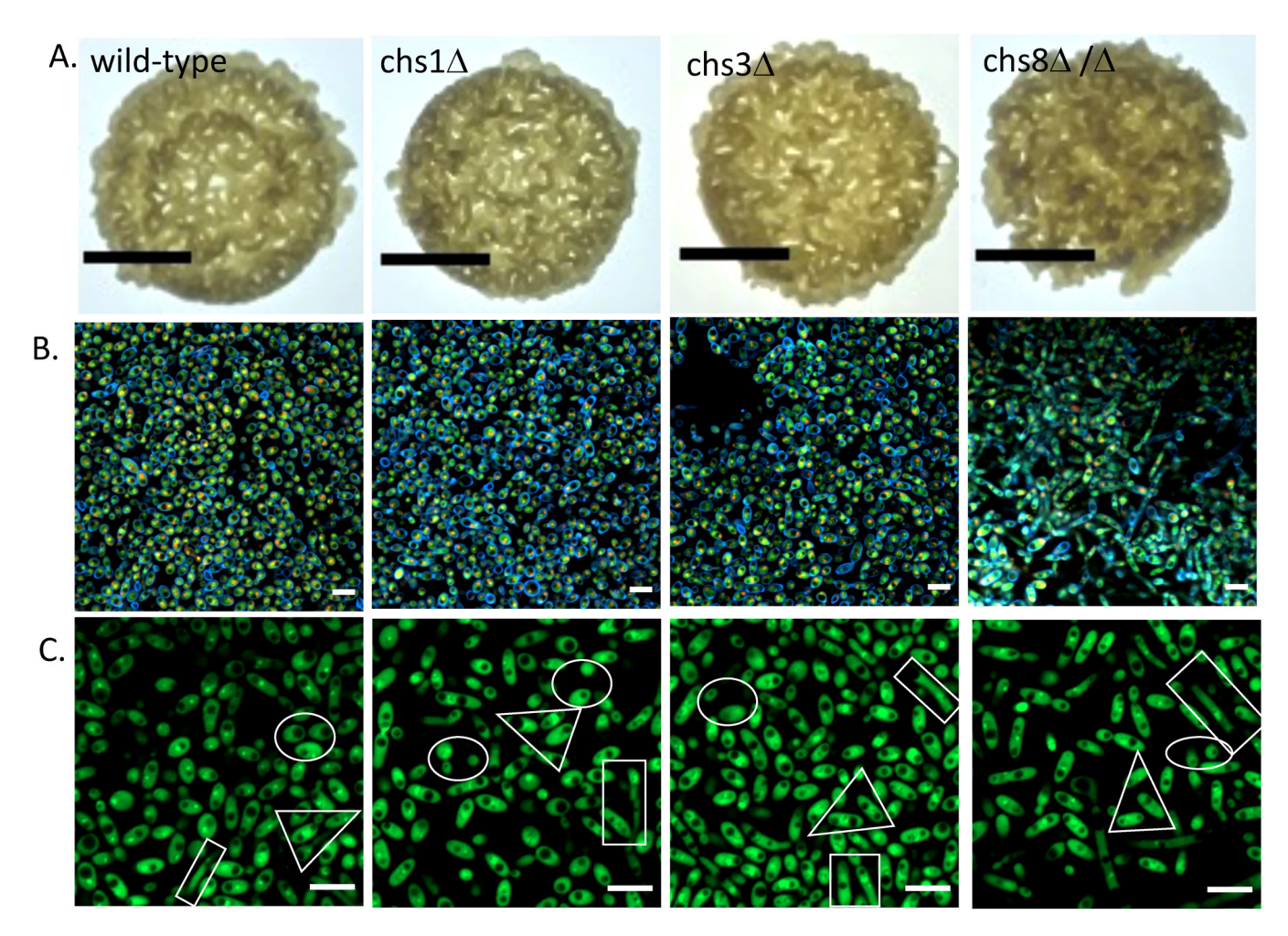
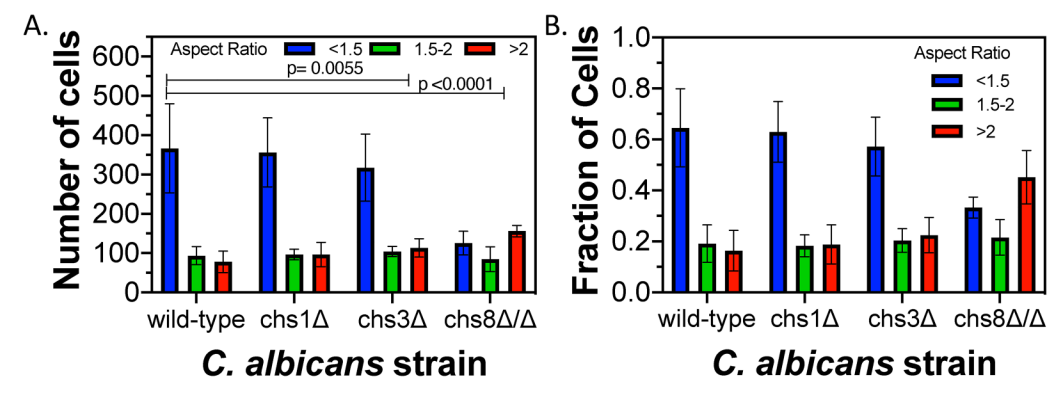


FIG. 11. Mutant morphology. (a) Representative photographs of *C. albicans* biofilms after 2 weeks of growth for each of the chitin synthase mutants used in the study. Scale bars are 5 mm. (b) Representative confocal microscopy images of the chitin synthase mutant biofilms. Blue is Calcofluor White straining the cell membrane and Green/Red is FUN-1 cytoplasm stain. Scale bar is 10 μm. (c) Representative confocal microscopy images of the chitin synthase mutant biofilms used for image analysis. Examples of yeast, pseudohyphae, and hyphae are designated with circles, triangles, and boxes, respectively. Scale bar is 10 μm.

[Fig. 13(b)], as well as the elastic stress as a function of strain amplitude [Fig. 13(c)]. Figure 14 details key rheological differences of the mutant biofilms. The  $chs1\Delta$  mutant had a larger linear elastic modulus [Fig. 14(a)] than both the wild-type and  $chs8\Delta\Delta\Delta$  (P=0.0013 and P=0.0018, respectively). The  $chs8\Delta\Delta\Delta$  mutant had a larger onset of

nonlinearity strain [Fig. 14(b)] than  $chs1\Delta$  (p=0.036) and  $chs3\Delta$  (p=0.019). There were no statistical differences in the yield stress calculated by the maximum value of the product  $G'\gamma_0$  [Fig. 14(c)]. Finally, the critical yield strain [Fig. 14(d)] of the wild-type biofilm was larger than all three mutants with *P*-values of 0.0039, 0.0012, and 0.0041 for  $chs1\Delta$ ,



**FIG. 12.** Cell counts. Quantification of the number (a) and fraction (b) of each cell shape present in *C. albicans* biofilm samples. Cells with an aspect ratio of <1.5 are classified as ovoidal yeast cells, an aspect ratio in the range 1.5–2.0 are labeled as elongated ellipsoidal pseudohyphae, and an aspect ratio of >2.0 are identified as filamentous hyphae. Error bars are standard error of the mean. *P*-values calculated from  $\chi^2$  testing of the mutant strain compared to wild type.

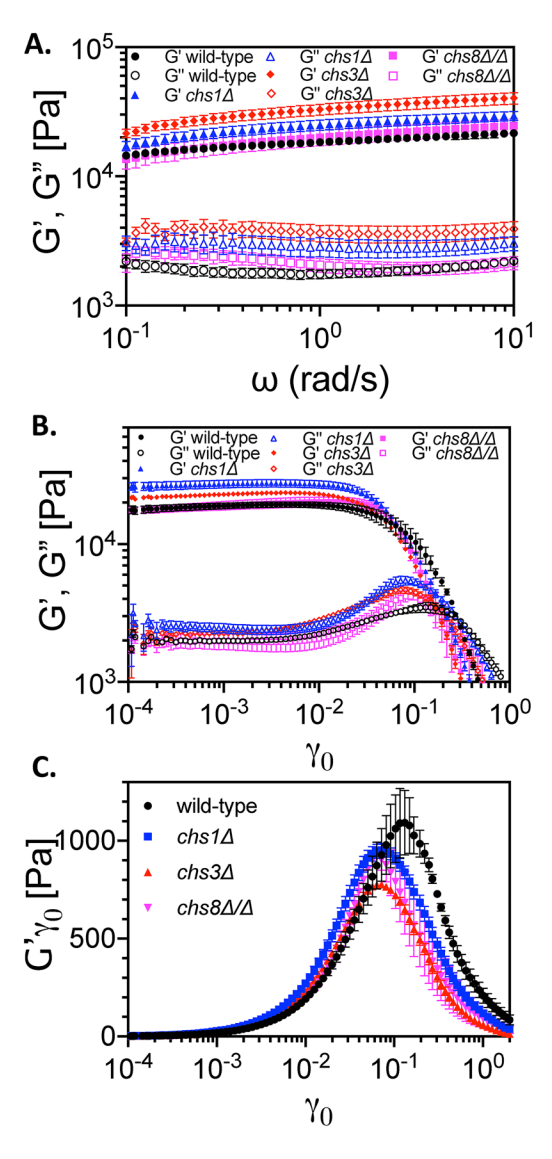


**FIG. 13.** Frequency sweeps, strain sweeps, and elastic stresses of mutant biofilms. Storage and loss moduli (G', G'') of *C. albicans* as a function of (a) frequency  $\omega$  at  $\gamma_0 = 0.0008$  and (b) strain at  $\omega = 1$  rad/s. These data include the average of four replicates. Error bars are standard error of the mean. (c) Elastic stress  $(G'\gamma_0)$  plotted as a function of strain amplitude. The intersection point (b) and the maximum of the curve (c) are taken to be the yield stress in each graph.

 $chs3\Delta$ , and  $chs8\Delta/\Delta$ , respectively. All *P*-values were calculated by one-way ANOVA with multiple comparisons. A summary of the key rheological properties for each mutant can be found in Table S4 in the supplementary material [55].

### IV. DISCUSSION

This paper reported the structural and rheological properties of fungal biofilms. First, we described a method to grow fungal biofilms that allows measuring fundamental linear and nonlinear rheological properties using parallel plate rheology. Next, we used an automated cell counting technique to classify dimorphic fungal cells in specimens based on the aspect ratio. Finally, we used these methods to describe three chitin synthase mutants of *C. albicans*. We show that it is possible to measure statistically significant differences in rheological properties; this method has utility in describing the

variability of phenotype in fungal biofilms. The rheological characterization is supported by measurements that found minimal effects in sample size, gap dependency, and evaporation.

These biofilms display interesting material structures that extend across multiple scales. Submillimeter voids and strands were observed by microscopy; these structures may hypothetically impact rheological properties. Using microscopy and image analysis, it would be beneficial to quantify the distribution of these features and correlate their size and shape with rheological properties. Quantitative characterization of these voids and strands, which could be accomplished by, e.g., confocal microscopy or microcomputed tomography, would furthermore complete a sequence of measurements of the biofilm morphology extending from macrostructure to microstructure. It is also possible that this macrostructural configuration could be affected by gene or environmental regulation; the substrate-normal dependence of the void and strand function could also be related to the spatial dependence of nutrient availability.

Given the new ability to characterize fungal biofilm rheology as reported in this article, we can compare the properties of this material with those of bacterial biofilms. The elastic modulus of this fungal biofilm— $18400 \pm 1100 \,\mathrm{Pa}$ —is on the high end of those reported for biofilms comprised of common bacteria species. For comparison, the G' for some common bacterial biofilm strains measured by parallel plate rheology are as follows: P. aeruginosa 200–3000 Pa [18,19]; S. epidermidis ~10 Pa [8]; B. subtilis ~2500 Pa [19]; and Comamonas denitrificans ~35 800 Pa [19]. Another rheological study of a mixed-species fungal biofilm found in the apple juice industry found that a biofilm made from Rhodototula mucilaginosa, Candida krusei, Candida kefyr, and Candida tropicalis, grown under static and turbulent flow conditions, had an elastic modulus of approximately 10<sup>4</sup> Pa [34], which is comparable to the values found in the present study.

In addition to the rheological characterization, we presented an automated method for describing the phenotypic cell shapes present in fungal biofilms. The aspect ratio has been used to characterize fungi phenotypical morphology previously; however, it was limited to hand counting of about 200 cells [32]. By automating the process using image analysis tools, we can characterize aspect ratios for thousands of cells in a matter of minutes. This increase would allow the investigation of other environmental parameters or gene mutations that may impact the phenotypical cell morphology of the fungal biofilm being studied. These phenotypes could have consequences for rheological properties.

This study investigated one possible contributor to fungal biofilm structure, chitin synthase. We demonstrated that we could distinguish differences between the chitin synthase mutants by counting cells based on the aspect ratio and measuring rheological properties. While we note that statistical differences were resolvable, we did not discover trends or correlations between cell shape, mutant strain, or rheological properties. This inability to make correlative statements suggests that chitin synthase's effect on the biofilm's structural properties is multifaceted and more investigation is necessary.

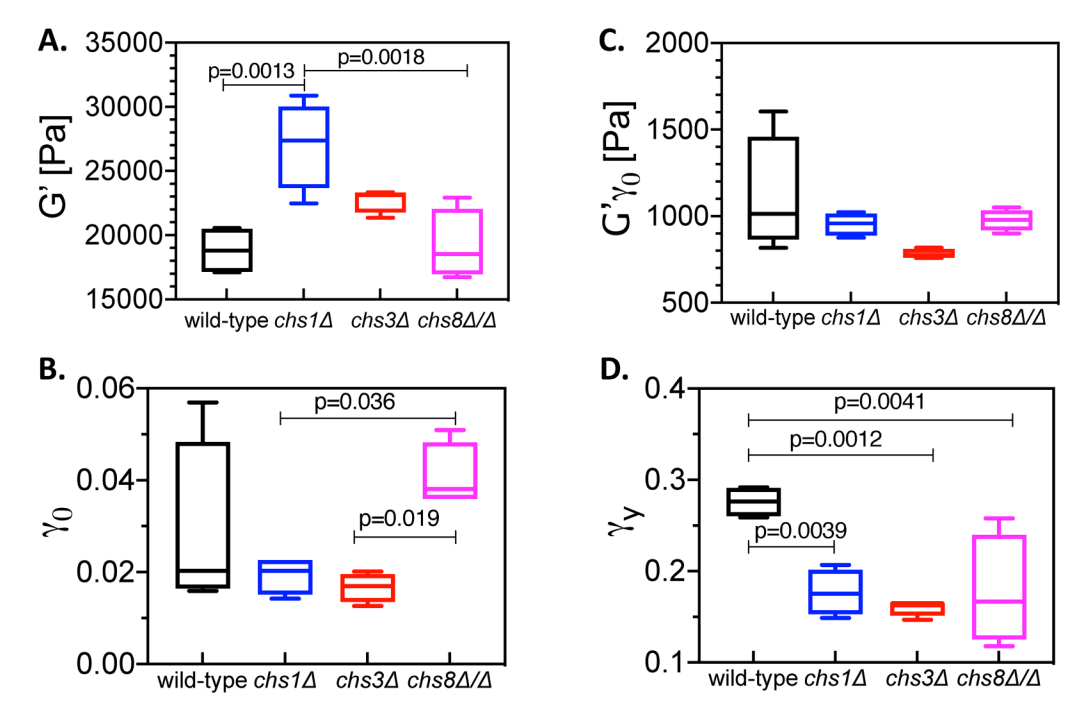


FIG. 14. Key rheological properties of mutant biofilms. (a) Average linear elastic modulus (plateau value), (b) onset of nonlinearity strain, (c) yield stress, (d) critical yield strain for wild-type,  $chs1\Delta$ ,  $chs3\Delta$ , and  $chs8\Delta/\Delta$  biofilms of *C. albicans*. Each box represents four sample replicates. *P*-values calculated by one-way ANOVA.

In future work using these mutants, factors that could be studied because of their potential impact on the biofilm structure include how much chitin is present in the biofilm and its distribution within the biofilm. Other factors that influence biofilm formation—such as cell rigidity, EPS composition, intercellular, matrix, and surface interactions-could also be explored. Returning to the specific question of how the mutations could generate rheological changes, these could be mediated by physicochemical effects originated by modifications in chitin synthase activity. Depending on the gene mutation, these activity changes are localized to different places in the fungal cell wall (cf. Table I). Variable chitin composition in the fungal wall could potentially affect cell flexibility as well as surface properties of the cell wall. The latter could lead to differences in both specific and nonspecific binding interactions with other cells or with the biofilm EPS. Such cell-EPS interactions have, for example, been implicated in the rheological properties of bacterial biofilms [6]. Additionally, the adhesion of *C. albicans* biofilms to plastic surfaces is decreased upon treatment with chitinase, an enzyme that degrades chitin. This observation is consistent with a role of cell wall chitin in affecting biofilm properties [50]. If the fungal biofilm rheological response is conceptualized as arising from either cellular or EPS effects and their cross-interaction, the cell-EPS binding represents a cross-interaction. Such cross-interactions represent a nonlocal mechanism for the observed rheological effects. For example, a gene-induced change in cell morphology could generate a rheological effect through a change in the degree of cell–EPS binding. These binding events can, in turn, generate indirect cell-cell interactions as well as modifications to EPS microdynamics. To uncover such interactions, future work should characterize the properties of the EPS, including its water, polysaccharide, and protein composition. EPS and fungal cell binding could also be investigated.

To summarize, researchers have sought to understand biofilm rheology by connecting viscoelastic response—both linear and nonlinear—to properties of the microbial cells, the EPS, and the interactions between cells and EPS. For bacterial biofilms, this response is influenced by factors such as cell type [51], environmental factors [21,52], macro- and microstructure features [53,54], and the EPS composition [6]. A suite of analysis tools has been developed to study these factors in bacterial biofilms. This paper provides tools to extend this paradigm by identifying rheological and microstructural characterization methods that can be applied for fungal biofilms. We have demonstrated a way to measure rheological properties and to characterize the macro- and microstructures of fungal biofilms. We hope that these methods can be further applied to better understand the factors that influence biofilm rheological properties, particularly EPS composition and the interaction of EPS with fungal cells. Because the methods presented here can resolve differences between different mutant strains, they can be used to study the genetic and environmental determinants of fungal biofilm mechanics.

Our work has, therefore, described a method to grow fungal biofilms and characterize their rheology using parallel plate rheology. We have demonstrated the method's utility by measuring the modulus, yield stress, and creep viscosity of *C. albicans* fungal biofilms. The method was also used to differentiate between mutant strains of biofilms. This method can be used to better understand the growth and development of fungal biofilms as well as to characterize how environmental and genetic factors can influence biofilm material properties.

### **ACKNOWLEDGMENTS**

We thank and acknowledge Nebibe Mutlu for the creation of the *Candida albicans* chitin synthase deletion mutants. We thank the Andrej Lenert lab for the use of their stereomicroscope. This work was supported by the National Science Foundation (NSF) under Award No. 1902359 and a University of Michigan MCubed award.

#### **AUTHOR DECLARATIONS**

#### Conflict of Interest

The authors have no conflicts to disclose.

#### **REFERENCES**

- Donlan, R. M., "Biofilms: Microbial life on surfaces," Emerg. Infect. Dis. 8(9), 881–890 (2002).
- [2] Douglas, L. J., "Candida biofilms and their role in infection," Trends Microbiol. 11(1), 30–36 (2003).
- [3] Cavalheiro, M., and M. C. Teixeira, "Candida biofilms: Threats, challenges, and promising strategies," Front. Med. 5, 28 (2018).
- [4] Costerton, J. W., K.-J. Cheng, G. G. Geesey, T. I. Ladd, J. C. Nickel, M. Dasgupta, and T. J. Marrie, "Bacterial biofilms in nature and disease," Annu. Rev. Microbiol. 41, 435–464 (1987).
- [5] Wilking, J. N., T. E. Angelini, A. Seminara, M. P. Brenner, and D. A. Weitz, "Biofilms as complex fluids," MRS Bull. 36(05), 385–391 (2011).
- [6] Stewart, E. J., M. Ganesan, J. G. Younger, and M. J. Solomon, "Artificial biofilms establish the role of matrix interactions in staphylococcal biofilm assembly and disassembly," Sci. Rep. 5, 13081 (2015).
- [7] Stewart, E. J., D. E. Payne, T. M. Ma, J. S. VanEpps, B. R. Boles, J. G. Younger, and M. J. Solomon, "Effect of antimicrobial and physical treatments on growth of multispecies *Staphylococcal* biofilms," Appl. Environ. Microbiol. 83(12), e03483-16 (2017).
- [8] Pavlovsky, L., J. G. Younger, and M. J. Solomon, "In situ rheology of Staphylococcus epidermidis bacterial biofilms," Soft Matter 9, 122–131 (2013).
- [9] Rogers, S. S., C. Van Der Walle, and T. A. Waigh, "Microrheology of bacterial biofilms in vitro: Staphylococcus aureus and Pseudomonas aeruginosa," Langmuir 24(23), 13549–13555 (2008).
- [10] Stoodley, P., I. Dodds, J. D. Boyle, and H. M. Lappin-Scott, "Influence of hydrodynamics and nutrients on biofilm structure," J. Appl. Microbiol. 85, 19S–28S (1998).
- [11] Besemer, K., G. Singer, R. Limberger, A. K. Chlup, G. Hochedlinger, I. Hödl, C. Baranyi, and T. J. Battin. "Biophysical controls on community succession in stream biofilms," Appl. Environ. Microbiol. 73(15), 4966–4974 (2007).
- [12] Stoodley, P., R. Cargo, C. J. Rupp, S. Wilson, and I. Klapper, "Biofilm material properties as related to shear-induced deformation and detachment phenomena," J. Ind. Microbiol. Biotechnol. 29(6), 361–367 (2002).
- [13] Gloag, E. S., S. Fabbri, D. J. Wozniak, and P. Stoodley, "Biofilm mechanics: Implications in infection and survival," Biofilm 2, 100017 (2020).
- [14] Fabbri, S., D. A. Johnston, A. Rmaile, B. Gottenbos, M. De Jager, M. Aspiras, M. E. Starke, M. T. Ward, and P. Stoodley, "Streptococcus mutans biofilm transient viscoelastic fluid behaviour during highvelocity microsprays," J. Mech. Behav. Biomed. Mater. 59, 197–206 (2016).

- [15] Chew, S. C., B. Kundukad, T. Seviour, J. R. C. Van der Maarel, L. Yang, S. A. Rice, P. Doyle, and S. Kjelleberg, "Dynamic remodeling of microbial biofilms by functionally distinct exopolysaccharides," MBio 5(4), 1–11 (2014).
- [16] Beroz, F., J. Yan, Y. Meir, B. Sabass, H. A. Stone, B. L. Bassler, and N. S. Wingreen, "Verticalization of bacterial biofilms," Nat. Phys. 14(9), 954–960 (2018).
- [17] Yan, J., A. G. Sharo, H. A. Stone, N. S. Wingreen, and B. L. Bassler, "Vibrio cholerae biofilm growth program and architecture revealed by single-cell live imaging," Proc. Natl. Acad. Sci. 113, E5337–E5343 (2016).
- [18] Qi, L., and G. F. Christopher, "Rheological variability of *Pseudomonas aeruginosa* biofilms," Rheol. Acta **60**, 219–230 (2021).
- [19] Jana, S. S. G. V. Charlton, L. E. Eland, J. G. Burgess, A. Wipat, T. P. Curtis, and J. Chen, "Nonlinear rheological characteristics of single species bacterial biofilms," npj Biofilms Microbiomes 6, 19 (2020).
- [20] Yan, J. A. Moreau, S. Khodaparast, A. Perazzo, J. Feng, C. Fei, S. Mao, S. Mukherjee, A. Košmrlj, N. S. Wingreen, B. L. Bassler, and H. A. Stone, "Bacterial biofilm material properties enable removal and transfer by capillary peeling," Adv. Mater. 30(46), 1804153 (2018).
- [21] Stoodley, P., Z. Lewandowski, J. D. Boyle, and H. M. Lappin-Scott, "Structural deformation of bacterial biofilms caused by short-term fluctuations in fluid shear: An *in situ* investigation of biofilm rheology," Biotechnol. Bioeng. 65(1), 83–92 (1999).
- [22] Billings, N., A. Birjiniuk, T. S. Samad, P. S. Doyle, and K. Ribbeck, "Material properties of biofilms—A review of methods for understanding permeability and mechanics," Rep. Prog. Phys. 78(3), 036601 (2015).
- [23] Araújo, G. R. S., N. B. Viana, F. Gómez, B. Pontes, and S. Frases, "The mechanical properties of microbial surfaces and biofilms," Cell Surf. 5, 100028 (2019).
- [24] Gordon, V. D., M. Davis-Fields, K. Kovach, and C. A. Rodesney, "Biofilms and mechanics: A review of experimental techniques and findings," J. Phys. D: Appl. Phys. 50(22), 223002 (2017).
- [25] Sadava, D., H. C. Heller, G. H. Orians, W. K. Purves, and D. M. Hillis, "Fungi recyclers, pathogens, parasites, and plant partners," in *Life: The Science of Biology*, 8th ed. (Sinauer Associates Inc., Sunderland, MA, 2008), pp. 650–669.
- [26] Free, S. J., "Fungal cell wall organization and biosynthesis," in Advances in Genetics, edited by T. Friedmann, J. C. Dunlap, S. F. Goodwin (Academic Press, Waltham, MA, 2013), Vol. 81, pp. 33–82.
- [27] Mayer, F. L., D. Wilson, and B. Hube, "Candida albicans pathogenicity mechanisms," Virulence 4(2), 119–128 (2013).
- [28] Spellberg, B., K. A. Marr, and S. G. Filler, "Candida: What should clinicians and scientists be talking about?," in Candida and Candidiasis, 2nd ed., edited by R. A. Calderone, C. J. Clancy (ASM, Washington, DC, 2012), pp. 1–8.
- [29] Tarifa, M. C., D. Genovese, J. E. Lozano, and L. I. Brugnoni, "In situ microstructure and rheological behavior of yeast biofilms from the juice processing industries," Biofouling 34(1), 74–85 (2018).
- [30] Mitchell, A. P., "Dimorphism and virulence in Candida albicans," Curr. Opin. Microbiol. 1(6), 687–692 (1998).
- [31] Sudbery, P., N. Gow, and J. Berman, "The distinct morphogenic states of *Candida albicans*," Trends Microbiol. 12(7), 317–324 (2004).
- [32] Song, Q., C. Johnson, T. E. Wilson, A. Kumar, and M. Snyder, "Pooled segregant sequencing reveals genetic determinants of yeast pseudohyphal growth," PLoS Genet. 10(8), e1004570 (2014).
- [33] Christensen, G. D., W. A. Simpson, J. O. Anglen, and B. J. Gainorl, "Methods for evaluating attached bacteria and biofilms," in *Handbook of Bacterial Adhesion: Principles, Methods, and Applications*, 1st ed., edited by Y. H. An and R. J. Friedman (Springer Science & Business Media, New York), pp. 213–233.

- [34] Brugnoni, L. I., M. C. Tarifa, J. E. Lozano, and D. Genovese, "In situ rheology of yeast biofilms," Biofouling 30(10), 1269–1279 (2014).
- [35] Chandra, J., D. M. Kuhn, P. K. Mukherjee, L. L. Hoyer, T. McCormick, and M. A. Ghannoum, "Biofilm formation by the fungal pathogen *Candida albicans*: Development, architecture, and drug resistance," J. Bacteriology 9(18), 109–118 (2001).
- [36] Berman, J., and P. E. Sudbery, "Candida albicans: A molecular revolution built on lessons from budding yeast," Nat. Rev. Genet. 3(12), 918–931 (2002).
- [37] Chaffin, W. L., J. L. López-Ribot, M. Casanova, D. Gozalbo, and J. P. Martínez, "Cell wall and secreted proteins of *Candida albicans*: Identification, function, and expression," Microbiol. Mol. Biol. Rev. 62(1), 130–180 (1998).
- [38] Marcilla, A., E. Valentín, and R. Sentandreu, "The cell wall structure: Developments in diagnosis and treatment of candidiasis," Int. Microbiol. 1(2), 107–116 (1998).
- [39] Wilson, R. B., D. Davis, and A. P. Mitchell, "Rapid hypothesis testing with *Candida albicans* through gene disruption with short homology regions," J. Bacteriol. 181(6), 1868–1874 (1999).
- [40] Walther, A., and J. Wendland, "An improved transformation protocol for the human fungal pathogen *Candida albicans*," Curr. Genet. 42(6), 339–343 (2003).
- [41] Noble, S. M., and A. D. Johnson, "Strains and strategies for large-scale gene deletion studies of the diploid human fungal pathogen *Candida albicans*," Eukaryot. Cell 4(2), 298–309 (2005).
- [42] Chandra, J., P. K. Mukherjee, and M. A. Ghannoum, "In vitro growth and analysis of *Candida* biofilms," Nat. Protoc. 3(12), 1909–1924 (2008).
- [43] Ramage, G., K. Vande Walle, B. L. Wickes, and J. L. López-Ribot, "Biofilm formation by *Candida dubliniensis*," J. Clin. Microbiol. 39(9), 3234–3240 (2001).
- [44] Buscall, R., "Letter to the editor wall slip in dispersion rheometry," J. Rheol. 54(6), 1177–1183 (2010).
- [45] Ewoldt, R. H., M. T. Johnston, and L. M. Caretta, "Experimental challenges of shear rheology: How to avoid bad data," in *Complex Fluids in Biological Systems* edited by S. Spagnolie (Springer, New York, NY, 2015), pp. 207–241.

- [46] Hyun, K., S. H. Kim, K. H. Ahn, and S. J. Lee, "Large amplitude oscillatory shear as a way to classify the complex fluids," J. Nonnewton. Fluid Mech. 107(1–3), 51–65 (2002).
- [47] Walls, H. J., S. B. Caines, A. M. Sanchez, and S. A. Khan, "Yield stress and wall slip phenomena in colloidal silica gels," J. Rheol. 47(4), 847–868 (2003).
- [48] Yang, M-C, L. E. Scriven, and C. W. Macosko, "Some rheological measurements on magnetic iron oxide suspensions in silicone oil," J. Rheol. 30(5), 1015–1029 (1986).
- [49] Towler, B. W., C. J. Rupp, A. B. Cunningham, and P. Stoodley, "Viscoelastic properties of a mixed culture biofilm from rheometer creep analysis," Biofouling 19(5), 279–285 (2003).
- [50] Al-Fattani, M. A., and L. J. Douglas, "Biofilm matrix of *Candida albi-cans* and *Candida tropicalis*: Chemical composition and role in drug resistance," J. Med. Microbiol. 55(8), 999–1008 (2006).
- [51] Yannarell, S. M., G. M. Grandchamp, S.-Y. Chen, K. E. Daniels, and E. A. Shank, "A dual-species biofilm with emergent mechanical and protective properties," J. Bacteriol. 201 (published online 2019).
- [52] Pavlovsky, L., R. A. Sturtevant, J. G. Younger, and M. J. Solomon, "Effects of temperature on the morphological, polymeric, and mechanical properties of *Staphylococcus epidermidis* bacterial biofilms," Langmuir 31(6), 2036–2042 (2015).
- [53] Ganesan, M., E. J. Stewart, J. Szafranski, A. E. Satorius, J. G. Younger, and M. J. Solomon, "Molar mass, entanglement and association of the biofilm polysaccharide of *Staphylococcus epidermi-dis*," Biomacromolecules 14(5), 1474–1481 (2013).
- [54] Stewart, E. J., A. E. Satorius, J. G. Younger, and M. J. Solomon, "Role of environmental and antibiotic stress on *Staphylococcus epidermidis* biofilm microstructure," Langmuir 29, 7017–7024 (2013).
- [55] See supplementary material at <a href="https://www.scitation.org/doi/suppl/10.1122/8.0000427">https://www.scitation.org/doi/suppl/10.1122/8.0000427</a> for information pertaining to the effects of sandpaper grit size on rheological measurement, images of the biofilm samples pre- and post-rheological testing, the impact of silicon oil on biofilm samples over time, and the characteristic rheological values for multiple C. albicans mutant strains.